Journal of Molecular Modeling (2020) 26: 326
https://doi.org/10.1007/s00894-020-04564-5

ORIGINAL PAPER

Molecular modeling and computational study of the chiral-dependent structures and properties of the self-assembling diphenylalanine peptide nanotubes, containing water molecules

Vladimir S. Bystrov[1] · Jose Coutinho[2] · Pavel S. Zelenovskiy[3,4] · Alla S. Nuraeva[3] · Svitlana Kopyl[5] · Sergei V. Filippov[1] · Olga A. Zhulyabina[6] · Vsevolod A. Tverdislov[6]

Received: 9 July 2020 / Accepted: 7 October 2020 / Published online: 2 November 2020

Abstract

DFT (VASP) and semi-empirical (HyperChem) calculations for the L- and D-chiral diphenylalanine (L-FF and D-FF) nanotube (PNT) structures, empty and filled with water/ice clusters, are presented and analyzed. The results obtained show that after optimization, the dipole moment and polarization of both chiral type L-FF and D-FF PNT and embedded water/ice cluster are enhanced; the water/ice cluster acquire the helix-like structure similar as L-FF and D-FF PNT. Ferroelectric properties of tubular water/ice helix-like-cluster obtained after optimization inside L-FF and D-FF PNT and total L-FF and D-FF PNT with embedded water/ice cluster are discussed.

Keywords Diphenylalanine · Peptide nanotube · Water molecules · Molecular modeling · DFT · Semi-empirical methods · Self-assembly · Polarization · Chirality

Introduction

Self-assembly of complex molecular structures based on amino acids (AA) is one of the most important phenomena both in living nature and in artificial biomimetics [1, 2]. At the same time, the chirality of the initial molecules also plays an important role in self-assembly processes [3, 4]. All this is important both for our understanding of wildlife and the basic principles of the emergence of life, and for numerous practical applications [5–7], including for biomedicine and targeted drug delivery [8, 9].

A necessary research approach here is computer molecular modeling of the processes of self-organization of molecular systems at the different levels and by different methods [10–12]. All AA have their own dipole moments [13], which interact with each other and self-organize into more complex molecular and crystalline structures, such as peptide nanotubes (PNT) and similar nanostructures [14]. Many of these structures have piezoelectric and ferroelectric properties [15–20]. This has been shown and investigated in detail in our work [20–26]. Self-assembly of such PNT occurs in aqueous media rather quickly and under certain conditions that affect the rate of their growth, the shape of self-organizing structures, and their structural and physical properties turn out to be significantly dependent on the chirality of the original molecules of amino acids and dipeptides [25–28]. In many cases, water molecules also appear in the internal hydrophilic cavity of such PNT [25–32]. They affect the physical properties of PNT and largely determine their changes. However, the experimental detection of water molecules by

✉ Vladimir S. Bystrov
vsbys@mail.ru

1 Institute of Mathematical Problems of Biology, Keldysh Institute of Applied Mathematics, RAS, 142290 Pushchino, Moscow region, Russia

2 Department of Physics & I3N, University of Aveiro, Campus Santiago, 3810-193 Aveiro, Portugal

3 School of Natural Sciences and Mathematics, Ural Federal University, Ekaterinburg 620000, Russia

4 Department of Chemistry & CICECO-Aveiro Institute of Materials, University of Aveiro, 3810-193 Aveiro, Portugal

5 Department of Physics & CICECO-Aveiro Institute of Materials, University of Aveiro, 3810-193 Aveiro, Portugal

6 Faculty of Physics, Lomonosov Moscow State University, 119991 Moscow, Russia

X-ray diffraction methods is very difficult. It is computer simulation methods that play an important role in the identifying as hydrogen atoms (protons) and these water molecules [33] and establishing their structural and physical properties, the effect on the properties of PNT as a whole. Computer molecular modeling allows one to calculate, investigate, and predict the basic physical properties of these nanostructures based on various AA.

In this paper, we focus on the further study of the structural and physical (including polar and ferroelectric-like) properties of PNTs based on FF (FF PNTs) of both different chirality L-FF and D-FFs and having embedded molecular clusters of water in the PNT's internal hydrophilic cavity. An optimum possible number of water molecules per one unit cell of the D-FF and L-FF hexagonal crystal structures (and for the D-FF and L-FF PNTs with minimum 2 coils of the PNT helix structure [21, 22, 24], corresponding to the period of a hexagonal unit cell along c-axis) were determined. The influences of these water molecules on the PNT's properties are analyzed, including a change in the dipole moments and polarization of the PNTs, as well as a change in the structure and properties (dipole moment and polarization) of water clusters embedded in a PNT cavity of both chirality types.

In all calculations, the quantum semi-empirical AM1, PM3, RM1 methods in the Hartee-Fock approximations (from HyperChem package [34]) are used. The initial structural data of D-FF and L-FF from the crystallographic database [35] were taken, and the DFT methods (in VASP program [36]) are applied, taking into account the van der Waals interactions (VdW correction by "PBE + D3" method). The results in comparison with known and experimental data are analyzed.

Initial models and main computational details

All main calculations were carried out, firstly, using density functional theory (DFT), as implemented by the Vienna Ab initio Simulation Package (VASP) [36–38]. The exchange −correlation potential was evaluated using the generalized gradient approximation (GGA) according to Perdew, Burke, and Ernzerhof (PBE) [39, 40]. Core states were described by means of the projector augmented wave method [41], while the Kohn−Sham problem (when calculating the energies of the ground states of systems) was addressed by using plane waves with kinetic energy up to Ecut = 400 eV to expand the wave functions.

In the calculations of self-assembled systems based on amino acids, it is also necessary to take into account the Van der Waals (VdW) interactions. Usual local and semilocal density functionals are unable to describe correctly Van der Waals interactions resulting from dynamical correlations between fluctuating charge distributions. A useful pragmatic method to work around this problem is to add a correction to the conventional Kohn-Sham DFT energy. In this paper, we have chosen a fairly reliable method for VdW correction named as D3, developed by Grimme, Stephan Ehrlich, and Helge Krieg [42]. This method is well compatible with PBE and is implemented in VASP (PBE + D3).

In this paper, further study of diphenylalanine peptide nanotubes is based on the models constructed from experimental data of their crystallographic structures obtained by X-ray methods and recorded in the crystallographic database of the Cambridge Crystallographic Data Center (CCDC) [35]. These data correspond to no. CCDC 16337 for L-FF [29] and No. CCDC 1853771 for D-FF [21, 25]. These structural data and visual models of both PNT L-FF & D-FF structures are easily reproduced in accordance with their periodic crystallographic cell parameters (Table 1) in the source files of modeling and calculations based on DFT methods in the VASP program [36] (Fig. 1).

The initial and water-free crystal structures of both L-FF and D-FF PNT types are shown on Fig. 1. The anhydrous and non-centrosymmetric hexagonal unit cell for both enantiomers crystal structures contains six FF molecules, and it is formed by a total of 258 atoms, while the space groups of these enantiomers are different: $P6_1$ space group for L-FF and $P6_5$ for D-FF. These initial crystal configurations were obtained from X-ray experimental CCDC data [35]. In all cases, the Brillouin zone (BZ) was sampled using a Monkhorst–Pack [44] scheme with a 1 × 1 × 3 mesh k-point sampling. The Hartree-Fock exact exchange was evaluated using the same k-point grid computed for the DFT potential. This enables a real-space grid of 120 × 120 × 28 points to keep along a1, a2, and a3 lattice vectors, respectively, which corresponds to the experimental lattice constants a1 = a2 = $a = b \sim$ 24 Å and a3 = $c = \sim$ 5.44 Å of the D-FF crystal structures data (Table 1). The relevant grid density appears to be about 5 points/Å along all the three directions.

The relaxation (optimization of the total energy) of both initial structures was carried out and the same procedure was also performed for all cases of simulated structures with different numbers of water molecules in the cavity of the inner channel of the nanotubes.

Table 1 Lattice cell parameters for L-FF and D-FF PNT (from [21, 25, 29] according to CCDC [35])

	L-FF	D-FF
Temperature	150 K	140 K
Space group	$P6_1$	$P6_5$
a, Å	24.0709(13)	23.9468(14)
b, Å	24.0709(13)	23.9468(14)
c, Å	5.4560(4)	5.4411(2)
V, Å^3	2737.7(3)	2702.2(2)
D, g/m^3	1.299	1.281

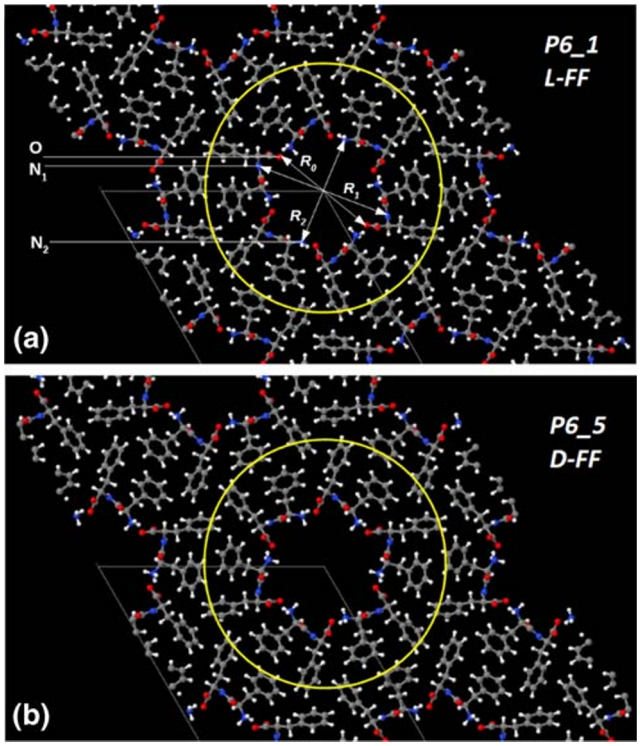

Fig. 1 Images of structures based on the Cambridge Crystallographic Data Center (CCDC) for two different FF enantiomers with symmetry elements (obtained using Jmol after performing VASP calculations) for cases: **a** L-FF with space group $P6_1$ and **b** D-FF with space groups $P6_5$. Hexagonal cells are marked by thin lines. Selected atoms and molecules for the formation of PNT are shown by a circle in yellow lines. Atoms are marked with colors: oxygen, red; nitrogen, blue; carbon, gray; hydrogen, white. The upper figure **a** shows the distances in the inner cavity: R_0, between the oxygen atoms O...O; R_1, between the nitrogen atoms N_1...N_1 (larger "far" diameter PNT); R_2, between the nitrogen atoms N_2...N_2 of the opposing NH_3^+ groups (short "near" inner diameter PNT) [43].

The relaxation cycle was stopped when the maximum force acting on lattice vectors and ions became less than 10 meV/Å.

The influence of water molecules on D-FF and L-FF PNT properties was studied with the use of the hexagonal ***Ih*** ice cluster model [45] which served as the basis for the construction of the initial model of a water cluster with different numbers n of water molecules (in the case of small n*(H_2O) water clusters with $n = 2$, 4, 6, etc., only a short part of such ***Ih*** ice cluster was used). The model clusters constructed were introduced into the cavity of the original anhydrous nanotubes, as was done in our earlier work [22]. Then, the whole D-FF and L-FF PNT structures, filled with this embedded water/ice cluster with n water molecules, were optimized, keeping the lattice parameters a, b, and c, of the initial nanotubes constant (Table 1). This is necessary to obtain a correlation with the initial experimental data. The obtained optimized structures with different numbers of water molecules in their cavity were collected and stored for further analysis of their parameters and visual control using different methods.

To estimate the energy of water molecule interaction with PNT and that of water binding inside PNT for each optimized structure with different quantities of water molecules n, we calculated a change in the total energy as the number of water molecules (average binding energy per FF unit cell as a function of the number of water molecules) increased:

$$E_b = E_{tot} - E_{PNT} - n \cdot E(H_2O) \quad (1)$$

where E_{tot} is the total energy per unit cell for the optimized PNT structure with water molecules, E_{PNT} is the energy of the optimized PNT structure without water molecules, $E(H_2O)$ is the energy of a relaxed single water molecule H_2O, and n is the number of H_2O molecules used in the calculation.

To determine changes in the main distances (R_o, R_1, R_2) inside the PNT cavity after relaxation and optimization of all the structures, we use Jmol software tool for visual presentation of all the structures extracted after calculations. For extraction of all atomic files and transformation of their formats, the OpenBabel and Cyberduck software tools were used too.

To obtain the values of the dipole moment, cluster volume, and polarization of the computed and extracted molecular clusters (both L-FF and D-FF structures with and without water and individual extracted water clusters), the HyperChem package [34] was used, with various quantum-mechanical semi-empirical AM1, PM3, RM1 methods (mainly in restricted Hartree-Fock (RHF) approximation) and some others necessary software tools.

Results and discussion

To identify the presence of water molecules and find their number, the PNT structures (both D-FF and L-FF chirality) with different numbers of water molecules were calculated and optimized. As result, optimized PNT models containing different number of water molecules in the inner cavity of the PNTs were obtained, and the dependence of PNT properties on the number of water molecules was studied.

Note that optimizing L-FF PNT with water is concerned with difficulties since these structures are less stable compared to D-FF PNT. This also agrees with previously obtained data: D-FF nanotubes have a denser and stronger deep packing than L-FF PNT [21, 24, 25]; L-FF PNT have larger cavity sizes, with looser and less uniform surface of the internal cavity compared to D-FF PNT [24, 26]. It was necessary to vary some parameters and methods of optimization procedure in VASP, to obtain the most stable and suitable optimized structure. These calculations require more time to proceed on a computer cluster. Nevertheless, finally, it was possible to obtain a good number of optimized structures for both D-FF and L-FF (albeit with slightly variations in their structural parameters, but sufficient to estimate reliably the effect of different

amounts of water molecules on the properties of the nanotubes) and choose the better ones for further analysis.

As a result, the dependences of the average binding energy E_b (1) per one unit cell FF as a function of the number of water molecules n were obtained for both types of structures L-FF and D-FF PNTs, convincingly showing that the minimum of this energy E_b is observed for $n = 21$ (Fig. 2). The peculiarity of the behavior of these dependences, the values, and position of the minimum of energies turned out to be similar to the data [32] and are comparable in magnitudes (see Fig. 3 in [32]).

The calculated mean binding energy E_b is the energy of an interaction between the water molecules and the inner wall of the nanotube through hydrogen bonds (HBs) [46, 47]. The formation of numerous hydrogen bonds (a network of hydrogen bonds) between water molecules and the nearest hydrophilic oxygen and nitrogen atoms on the inner surface of the nanotube cavity (including with NH_3^+ groups) was found in all the optimized structures obtained for nanotubes of both types of chirality L-FF and D-FF. This is also clearly demonstrated by the HyperChem-built images of optimized structures extracted from the VASP (as shown Figs. 4, 5, and 6 and discussed in greater detail below).

These results are also confirmed by the calculated dependences of the internal diameters of the nanotube cavity, determined by the distances between the main nitrogen atoms N_1, N_2: $R_1(N_1\text{-}N_1)$ and $R_2(N_2\text{-}N_2)$ (determined in Fig. 1a). As the number of water molecules n increases, the size of the inner PNT cavity changes for both types of chirality L-FF and D-FF. Comparing calculated and experimental values of R_1 and R_2, we can see that when the number of molecules is equal to $n = 21$, the calculated curves intersect with the experimental values, which are according to X-ray structural data for the initial nanotubes (data in Table 2), for both L-FF and D-FF PNTs.

These graphs (Fig. 3a, b) show that $n = 21$, the obtained curves of the dependencies of the internal dimensions of the cavities of the optimized structures of the nanotubes of both chiral types, coincides in very close sizes variations with the experimental data.

As a result, it can be argued that in the L-FF and D-FF cavities of both types of chirality, there are about $n = 21$ water molecules per unit cell of these FF periodic molecular crystal structures.

Preliminary analysis showed that in all cases, water-ice clusters after optimization in the internal cavity of both types L-FF and D-FF PNT change their structure and properties, but of the greatest interest is the case with the found amount of 21 water molecules, which is corresponding to the minimum total energy of both types of chirality. Extraction of the optimized water cluster (with 21 H_2O molecules) from the inner cavity shows that this cluster has changed compared to the initial hexagonal ice structure and acquired a helix-like structure, close to the helix, which is typical for D-FF PNTs per se (see on Figs. 7, 8, and 9 and discussion below). Moreover, a water cluster splits into an inner part and an outer part, and the latter actively forms hydrogen bonds with the atoms of nitrogen and oxygen of the inner surface of the PNT cavity. It turns out also that after optimization, water molecules in the outer part (close to the inner PNT surface of the cavity) are located approximately in the middle between the layers of FF molecules. These data are partly confirmed by recent studies using the dielectric spectroscopy [48]. All these data need more deep and detailed analysis.

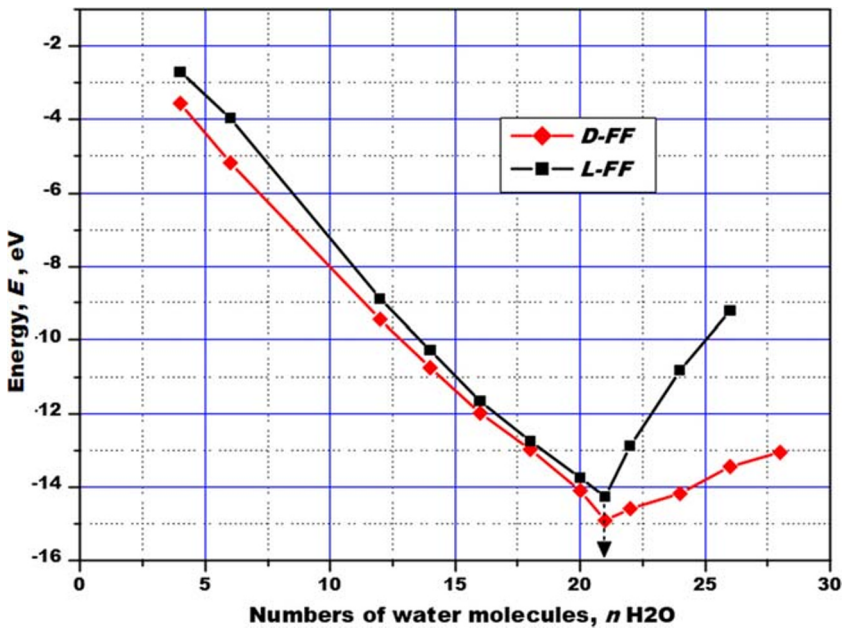

Fig. 2 Average binding energy E_b as a function of number of water molecules confined in the hydrophilic channel of FF PNT for each chirality types: L-FF and D-FF

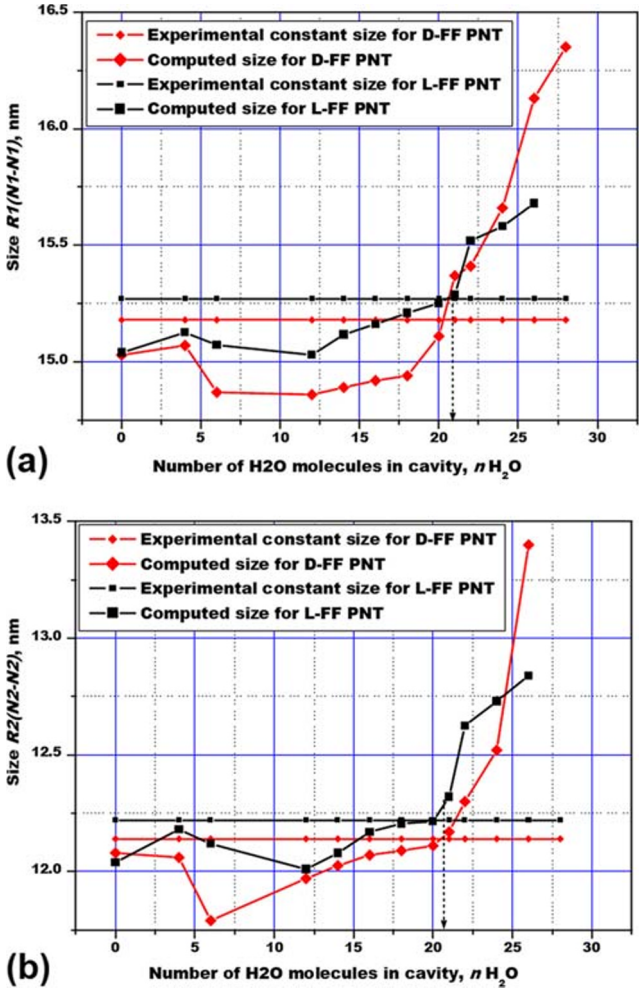

Fig. 3 Dependences of the internal cavity sizes of the optimized structures of nanotubes of both types of chirality L-FF and D-FF containing a different number of water molecules on the number *n* of these water molecules, in comparison with the known sizes of the internal sizes of nanotubes according to experimental data (Table 2) [25, 29, 35]. **a** R_1, between the nitrogen atoms $N_1...N_1$ (larger "distant" diameter PNT); **b** R_2, between the nitrogen atoms N2…N2 of the opposite NH3 + groups (short "near" inner diameter PNT)

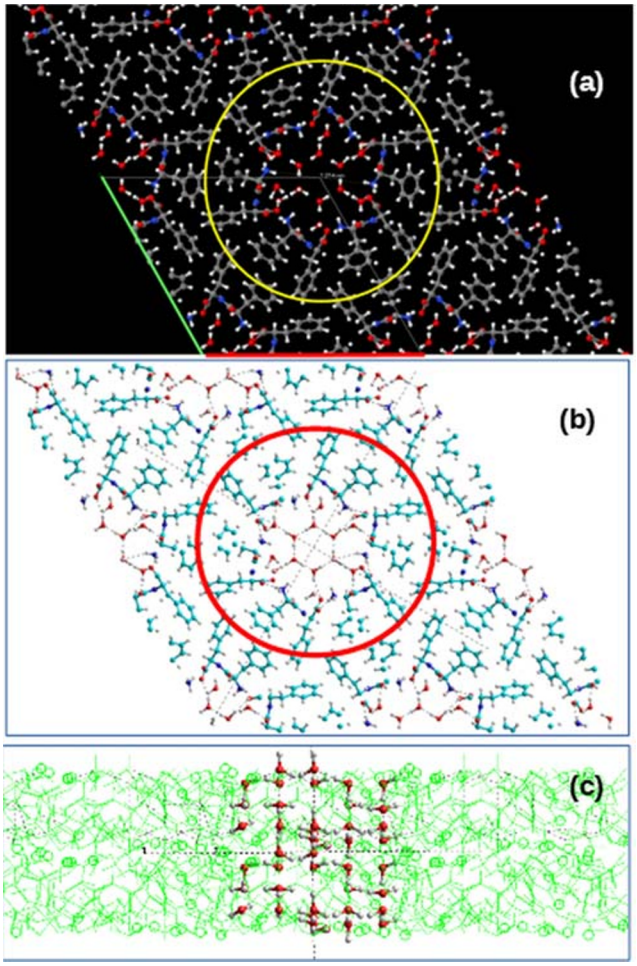

Fig. 4 Schematic images of the initial water cluster embedded into the inner hydrophobic hallow cavity of the D-FF PNT: **a** top Z-projection images consisting from 4 unit cells of D-FF crystal structure obtained using Jmol from VASP initial data before optimization calculations (green and red lines marked the unit cell; yellow circle shows the selected atoms and molecules that form the PNT with cavity in the center filled with water cluster molecules; the colors of atoms are the same as of Fig. 1); **b** the same Z-projection images converted from VASP to HyperChem workspace using Cyberduck and OpenBabel software (red circle shows the same selected atoms and molecules that form the PNT with cavity in the center filled with water cluster molecules; the colors of atoms here are as follows: carbon is cyan, red is oxygen, white is hydrogen); **c** side Y-projection and cross-section of D-FF structures with selected water molecules formed initial water cluster [43].

Water cluster structures details

Let us consider the structures of water clusters obtained with 21 H_2O molecules per a unit cell in greater detail. In this case, the initial water cluster based on the hexagonal ***Ih*** ice cluster models and consisting of 21 H_2O molecules per a unit cell is presented in Fig. 4 for the case of D-FF PNT. A similar initial structure is used for L-FF PNT. During the optimization process (using the VASP program, as described above), the structure of water clusters changes—there is a displacement of water molecules inside the cavity under the influence of an electric field inside the cavity (arisen from fixed FF dipoles, which create total strong polarization here and, accordingly, a strong electric field arises along the axis of the nanotube [20–25]). As noted above, we optimize only the structure of the water cluster inside a PNT cavity, keeping fixed (frozen) atomic positions of all the atoms of all the FF molecules and the unit cell parameters of the PNT crystal structures. In this case, a rearrangement of hydrogen bonds occurs both between water molecules and between water molecules and FF molecules (in particular, with nitrogen and oxygen atoms of FF molecules on the inner hydrophilic surface of the nanotube's cavity). This happens both in D-FF PNT and in L-FF PNT, but in different ways in accordance with their different internal structure and chirality. As a result, we get two altered and significantly different structures of water clusters after

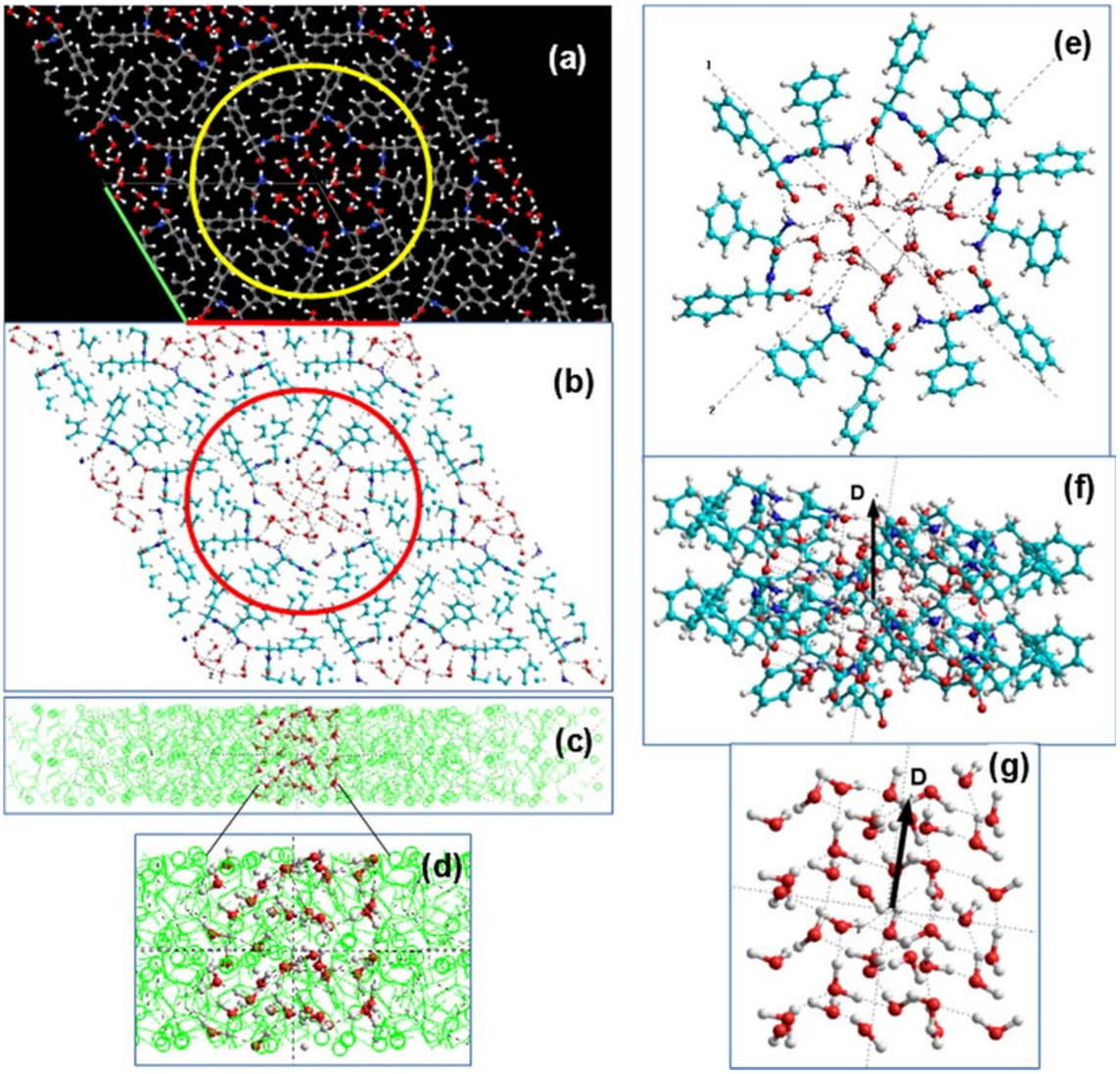

Fig. 5 Schematics of the D-FF PNT structures with optimized 21H2O per unit cell embedded water cluster (the designations used are the same as in Fig. 4 above): **a** Z-projection image from VASP computed data with 4 unit cell; **b** the same image converted into HyperChem workspace; **c** side Y-projection and cross-section of D-FF structures with selected water molecules formed initial water cluster; **d** inset with biggest image of water cluster; **e** Z-projection image of the D-FF 2 coils with 42H2O embedded water cluster; **f** Y-projection image of the D-FF 2 coils with $42H_2O$ embedded water cluster (D shows the total dipole momentum); **g** Y-projection image of the $42H_2O$ water cluster extracted from D-FF PNT after optimization (D shows the total dipole momentum for water cluster) [43].

their optimization in D-FF and L-FF chirality cases (Fig. 5 and Fig. 6).

The initial water cluster with 21 H_2O molecules constructed on the basis of a ***Ih*** hexagonal ice structure, in general, had a correct symmetrical organization and a small dipole moment directed on average perpendicular to the axis of the nanotube (see Tables 3 and 4). After optimization of this cluster embedded in the cavity of both PNT, its structure has changed. Moreover, this happened in different ways, depending on the type of the surrounding PNT structure. In both the cases (L and D), a distortion of the structure occurs with the formation of a strong dipole moment oriented along the PNT axis.

For a more detailed analysis, we transformed the optimized structures obtained from VASP into HyperChem workspace and distinguished between the models of the structures of both D-FF and L-FF PNTs themselves (consisting from two helix coils) and models of nanotubes containing 42 H_2O molecules each. These models correspond to 2 layers extracted from the VASP structures with a super-cell of their 4 initial crystal unit cells in plane (and $8 = 2 \times 2 \times 2$ unit cells total) for each D-FF and L-FF structures. Figures 5 and Fig. 6 schematically show the procedures for such transformations.

Then, we identified the structures of extracted water clusters themselves from the structures of nanotubes in the HyperChem workspace. This is also shown in Fig. 5 and Fig. 6.

Figure 7 shows 42 H2O water clusters, extracted from 2-coil PNTs (initial and optimized in the D-FF and L-FF PNT).

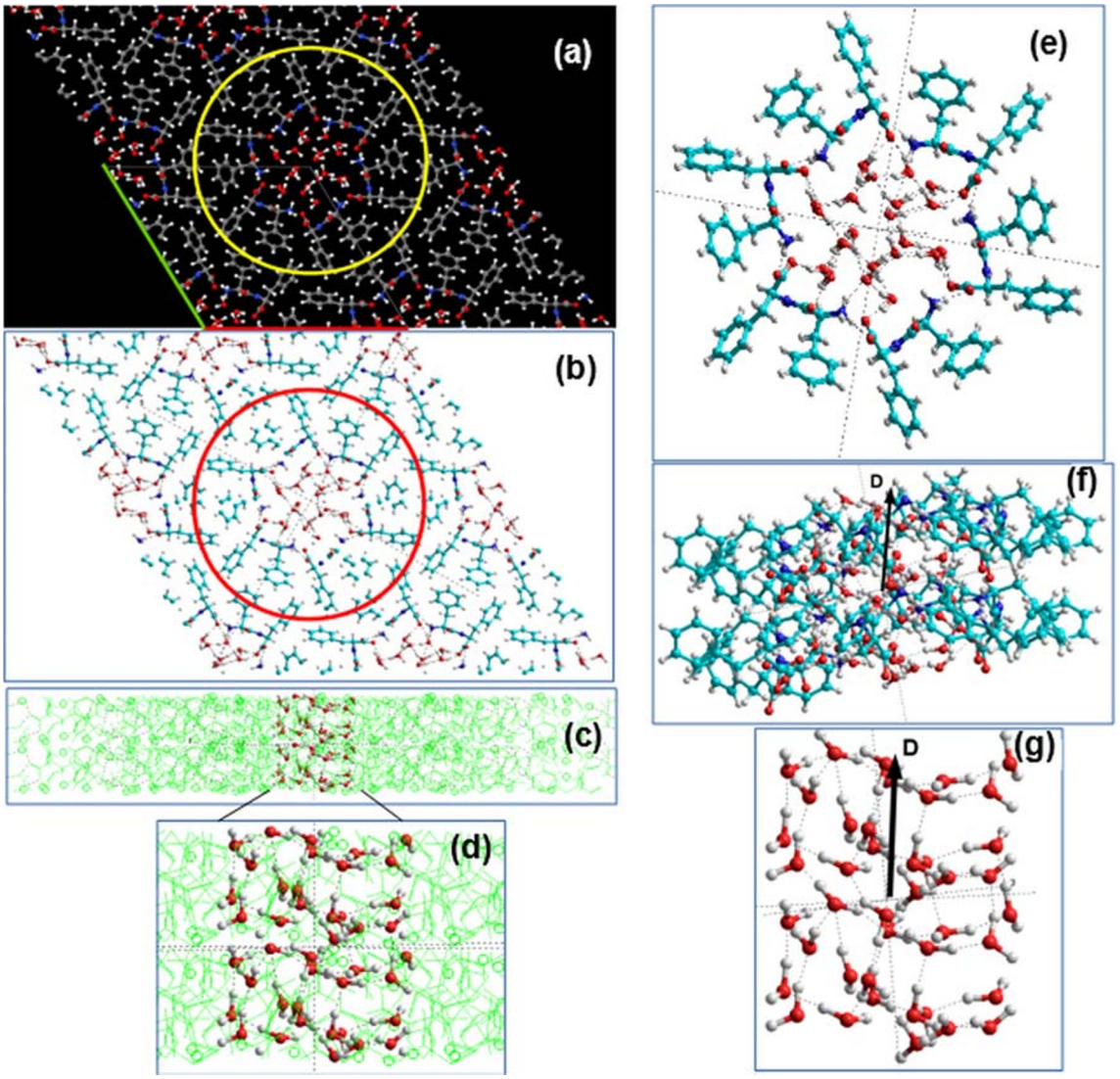

Fig. 6 Schematics of the L-FF PNT structures with optimized 21H2O per unit cell embedded water cluster (the designations used are the same as in Fig. 4 above): **a** Z-projection image from VASP computed data with 4 unit cell; **b** the same image converted into HyperChem workspace; **c** side Y-projection and cross-section of L-FF structures with selected water molecules formed initial water cluster; **d** inset with biggest image of water cluster; **e** Z-projection image of the L-FF 2 coils with 42H2O embedded water cluster; **f** Y-projection image of the L-FF 2 coils with $42H_2O$ embedded water cluster (D shows the total dipole momentum); **g** Y-projection image of the $42H_2O$ water cluster extracted from L-FF PNT after optimization (D shows the total dipole momentum for water cluster) [43]

Table 2 Parameters of inner hydrophilic cavity of L-FF and D-FF PNTs

Parameter	L-FF		D-FF	
	Initial	Opt (no water)	Initial	Opt (no water)
a, Å	24.0709	23.8308(284)	23.9468	23.7877(806)
b, Å	24.0709	23.8308(284)	23.9468	23.7877(806)
c, Å	5.4560	5.4035(861)	5.4411	5.4022(7125)
R_0, Å	12.236	12.091	12.102	12.075
R_1, Å	15.271(698)	15.042(076)	15.180(569)	15.030(688)
R_2, Å	12.218(349)	12.098(817)	12.135(396)	12.075(906)
Etot, eV	− 1593.31826706	− 1657.64346817	− 1608.7356382	− 1657.60024131

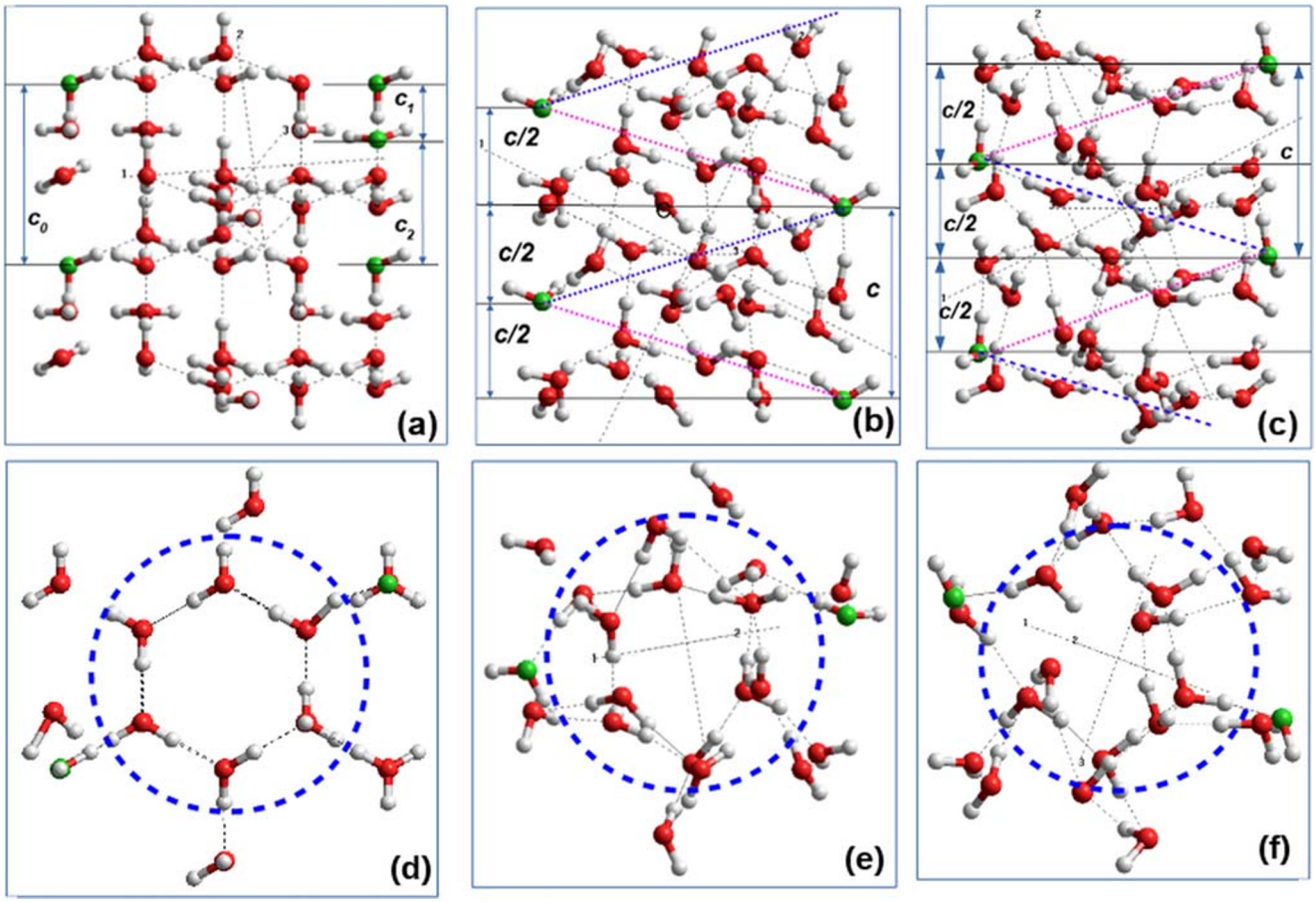

Fig. 7 Extracted 42H2O water clusters in Y-projection (**a**, **b**, **c**) and Z-projection (**d**, **e**, **f**): **a** and **d** for initial water cluster based on Ih structure; **b** and **e** after optimization in D-FF PNT; **c** and **f** after optimization in L-FF PNT. Dashed lines (with two colors) on **b** and **c** show different direction of the helix-like structure formation in D-FF PNT cavity and L-FF PNT cavity cases. Dashed circles on **d**, **e**, and **f** show difference between inner and outer water molecules groups. Parameters of periodical water clusters structures: **a** $c_0 = 5.434$ Å, $c_1 = 1.670$ Å, $c_2 = 3.764$ Å; **b** $c = 5.441$ Å; **c** $c = 5.456$ Å [43]

The main feature is that the shift of the individual water molecules is different for D-FF and L-FF PNT—they acquired a helix-like structure with a helix pitch equal to the period of the corresponding D-FF and L-FF PNT helix (that is equal to the period of their periodical crystal structure parameter *c*, see in Table 1). Figure 7 b and c, schematically shows various helix-like structures (in Y-projection) in comparison with the initial water cluster structure (Fig. 7a). Figure 7 d, e, and f shows a separation of the molecular groups of the water cluster into their internal (or inner) and external (or outer) sub-groups. The outer molecules interact actively with FF atoms on the inner hydrophilic PNT cavity surface, namely with nitrogen and oxygen atoms due to hydrogen bonds [43]. These results are also confirmed by Visual-Differential analysis [26], which are to be published in a separate article.

Polarization details

Let us now consider in greater detail the polar properties of both nanotubes with integrated water clusters and the water clusters themselves. In order to carry out calculations of polar properties, the calculation data obtained in VASP were converted into HyperChem medium workspace. This procedure was performed using the OpenBabel, Cyberduck, and HyperChem software [34]. Using these software, the optimized structures were transformed from periodical crystal D-FF and L-FF structures in VASP to HyperChem workspace as one, two, and more D-FF and L-FF coils helix molecular structures, where all further calculations were carried out. Furthermore, the optimized water cluster structures placed in D-FF and L-FF cavity was obtained too and was cut out from cavity to investigate independently. Schematic of main steps of these procedures was presented in Fig. 5 e, f, and g and Fig. 6 e, f, and g. For each structure investigated (initial D-FF and L-FF without water molecules inside, initial D-FF and L-FF with 21 water molecules per a unit cell, and finally optimized ones), quantum-chemical calculations were carried out using semi-empirical quantum methods [48, 49]: AM1, RM1, and PM3 in the restricted Hartree-Fock (RHF) approximation. The data obtained (energies, dipole momentum, polarizations) and

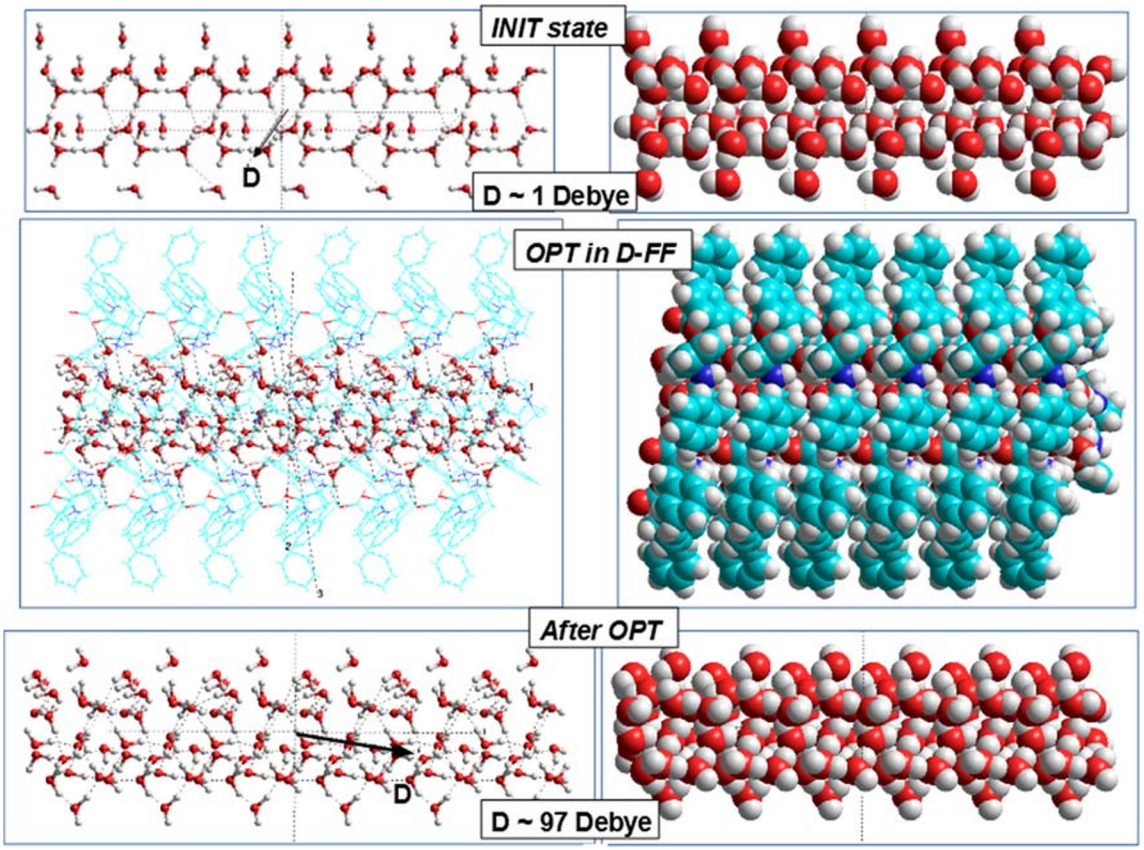

Fig. 8 Images of the water/ice tubular nanostructures and D-FF PNT with water inside cavity from 6 repeated coils along c-axis (in X-projection): **a** initial tubular water/ice structure; **b** D-FF PNT with embedded water/ice structures under optimization process; **c** water/ice tubular helix structure after optimization inside D-FF PNT; **d**, **e**, and **f** the same in the VdW surface presentation Vector **D** shows the direction of the total dipole momentum in the initial and optimized water cluster

the volumes of all molecular structures were presented in Table 3 and Table 4.

Accurate calculations are possible with HyperChem by using methods that neglect some, but not all, of the electron-electron interactions. These methods are called Neglect of Differential Overlap or NDO methods. These methods were further improved and developed by J. J. P. Stewart and co-workers [50–57]; they are based on the so-called neglect of diatomic differential overlap (NDDO) approximation, with several modifications and with the choice of a wide number of parameters enable one to reproduce experimental quantities. NDDO retains all one-center differential overlap terms when Coulomb and exchange integrals are computed. The NDDO approximation is the basis for the Modified Neglect of Diatomic Overlap (MNDO), AM1, and PM3 methods. AM1 (Austin Model 1) is a modified MNDO method proposed and developed by M. J. S. Dewar and co-workers at the University of Texas at Austin [50–52]. AM1 is generally the most accurate computational method and is often the best method for collecting quantitative information [50–52]. PM3 differs from AM1 only in the values of the parameters [53–55]. The parameters for PM3 were obtained by comparing a large number of experiments with calculation results. As a rule, non-covalent interactions in the PM3 method are less repulsive than in AM1. RM1 is other semi-empirical method which was parameterized to calculate dipole moments and enthalpies of formation, with errors smaller than those for AM1 and PM3 [56, 57]. Energetic properties of organic compounds can be calculated in both forms: isolated, and in solvent medium. All methods are available and provide close data for the biomolecular systems studied in this article based on C, O, N, and H atoms.

The main results obtained: (1) after optimization, the embedded water molecular cluster has a big own dipole moment strongly oriented along D-FF and L-FF PNT channel, while before it did not have such a defined orientation and a very small dipole moment (Figs. 5, 6 f and g, 8, and 9, and Tables 3 and 4); (2) the structure organization of both these water clusters after optimization inside D-FF and L-FF cavity has changed greatly—both have acquired helix properties, with the same helix step as D-FF and L-FF PNT (Fig. 7); and (3) the total dipole moment and polarization of both D-FF and L-FF PNT after optimization with embedded 21 H_2O water/ice clusters enhance in the direction of main c-axis of each PNTs (Tables 3, 4, and 5, Figs. 8 and 9).

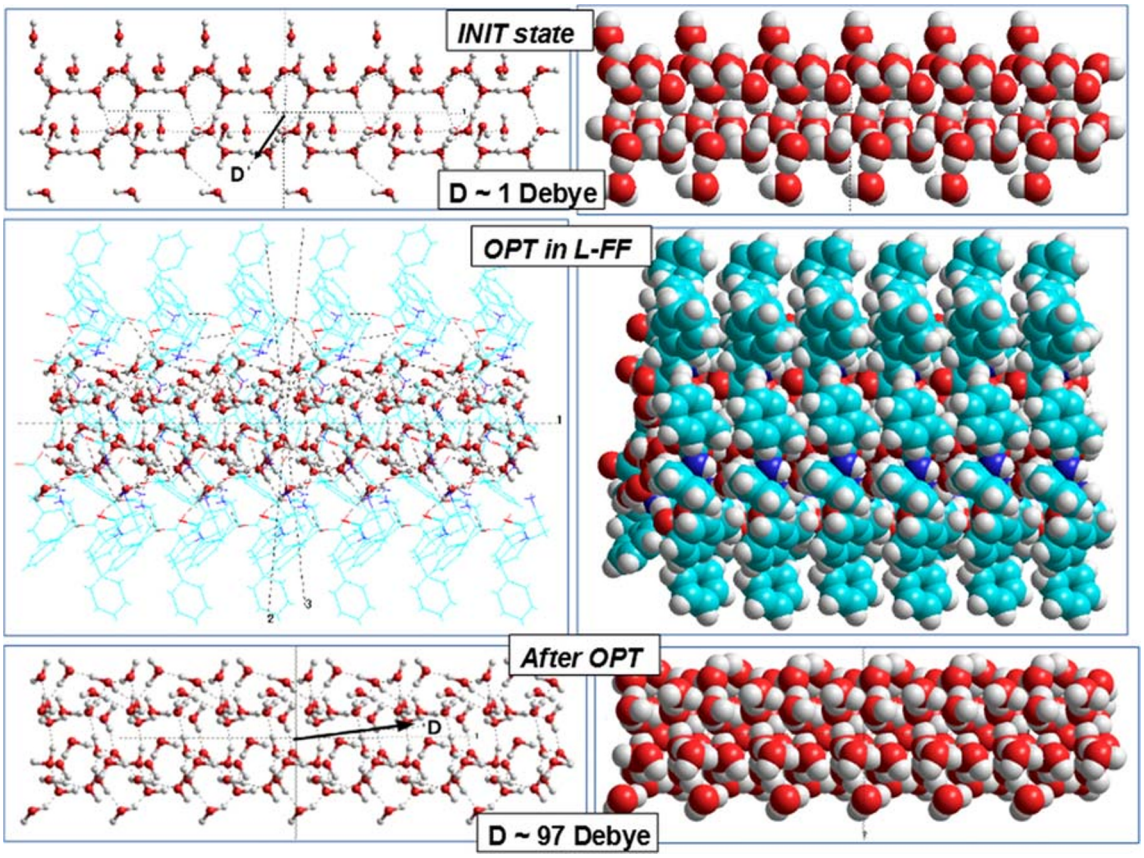

Fig. 9 Images of the water/ice tubular nanostructures and L-FF PNT with water inside cavity from 6 repeated coils along c-axis (in X-projection): **a** initial tubular water/ice structure; **b** L-FF PNT with embedded water/ice structures under optimization process; **c** water/ice tubular helix structure after optimization inside L-FF PNT; **d**, **e**, and **f** the same in the VdW surface presentation vector **D** shows the direction of the total dipole momentum in the initial and optimized water cluster

Table 3 Data of dipole moment and polarization of D-FF PNT and water clusters, computed using AM1 RHF method (HyperChem). Similar and close data are obtained by PM3 and RM1 methods

Data			D-FF 2 Coils		Water/ice cluster 21 H_2O in D-FF cavity		D-FF + 21 H_2O after optimization
			Without H_2O	With initial 21 H_2O	Initial 21 H_2O	21 H_2O after optimization	
Dipole, Debye	Dt		140.385	139.520	1.104	29.404	158.461
	Dz		− 140.349	− 139.447	− 0.876	− 28.385	− 158.441
Polariza-tion, C/m^2	VdW volume	Pt	0.1399274	*0.1194850*	0.005685	0.150753	*0.13321788*
		Pz	− 0.1398915	− 0.1194226	− 0.004511	− 0.1455383	− 0.13320106
	Solvent volume	Pt	*0.0590361*	*0.0540235*	0.001695	0.0510458	*0.06148752*
		Pz	*− 0.05902138*	*− 0.0539953*	− 0.001345	− 0.049277	*− 0.0614798*
Energy	Et, a.u.		− 1739.52560	− 2271.06543	− 534.5776	− 537.78035	− 2277.23035
	ΔEt, eV					− 87.151311	− 167.7561
	Eb, eV		− 2265.27936	− 2495.46785	− 312.84856	− 399.99734	− 2663.21967
	ΔEb, eV					− 87.14878	− 167.75182
Volume*) VdW	V, $Å^3$		3346.47	3894.86	647.80	650.55	3967.61
Volume**) solvent for 1.4 Å	V, $Å^3$		7931.75	8614.35	2172.99	1921.33	8596.16

*) This Van der Waals (VdW) volume is calculated by the VdW surface area (grid) calculation

**) This volume is calculated by solvent-accessible surface area calculations, specifies the effective radius of the solvent molecule (in Ångstroms) Generally, (and in this work too) a value of 1.4 Å is used for water as a solvent

Table 4 Data of dipole moment and polarization of L-FF PNT and water clusters, computed using AM1 RHF method (HyperChem). Similar and close data are obtained by PM3 and RM1 methods

Data AM1 RHF			L-FF 2 Coils		21 H_2O in L-FF cavity		L-FF + 21 H_2O after optimization
			Without H_2O	With initial 21 H_2O	Initial 21 H_2O	21 H_2O after optimization	
Dipole, Debye	Dt		140.757	133.110	1.104	28.646	157.8331
	Dz		− 140.217	− 130.279	− 0.876	− 28.386	− 157.035
Polariza-tion, C/m^2	VdW volume	Pt	0.139501	*0.113128*	0.005685	0.148244	*0.13252224*
		Pz	− 0.138966	− 0.110722	− 0.004511	− 0.146898	− 0.13185222
	Solvent volume	Pt	*0.0590361*	*0.0496268*	0.001695	0.0494868	*0.06073597*
		Pz	*− 0.05902138*	*− 0.0481101*	− 0.0013447	− 0.049038	*− 0.0604289*
Energy	Et, a.u.		− 1739.02739	− 2272.76298	−534.5776	− 537.68028	− 2278.81422
	ΔEt, eV					− 84.42816	− 164.66275
	Eb, eV		− 2251.72290	− 2541.65947	−312.84856	− 397.27426	− 2706.3170
	ΔEb, eV					− 84.42570	− 164.6573
Volume*) VdW	V, $Å^3$		3365.60	3924.73	647.80	644.55	3972.63
Volume**) solvent for 1.4 Å	V, $Å^3$		7931.75	8673.83	2172.99	1930.83	8668.04

*) This Van der Waals (VdW) volume is calculated by the VdW surface area (grid) calculation

**) This volume is calculated by solvent-accessible surface area calculations, specifies the effective radius of the solvent molecule (in Ångstroms) Generally, (and in this work too) a value of 1.4 Å is used for water as a solvent

Important feature is that after optimization inside D-FF and L-FF PNT cavity, the water/ice clusters acquired different directions of rotation of a helix. This property of helix lines is called chirality: "right chirality" (D from the Latin "dextra") and "left chirality" (L from the Latin "laeva"). Usually, such a pair of mirror-symmetrical helix lines are called enantiomorphs [21, 25, 58].

This last result (showing on Figs. 7, 8, and 9), concerned with very pronounced realignment of water cluster structure, is confirmed by some other important computed data. The

Table 5 Dipole moments and polarization for water/ice cluster after optimization in D-FF and L-FF PNT, consisting from 126 H_2O molecules (see on Fig. 8 and Fig. 9), computed by various methods

126 H_2O water/ice cluster after optimization			Method used (in RHF)					
			From D-FF			From L-FF		
			AM1	PM3	RM1	AM1	PM3	RM1
Dipole moment, Debye		Dt	95.920	97.355	100.575	94.982	97.226	99.533
		Dz	*− 93.496*	*− 95.058*	*− 98.130*	*− 94.653*	*− 96.787*	*− 99.154*
		Dy	*− 15.324*	*− 14.816*	*− 15.481*	*7.304*	*8.528*	*8.068*
		Dx	14.978	14.912	15.695	2.991	3.521	3.188
Polariza-tion, C/m^2	VdW V, $Å^3$		1927.21			1910.28		
	Volume VdW	Pt	0.1660	0.1685	0.1741	0.1655	0.1698	0.1738
		Pz	*− 0.1618*	*− 0.1645*	*− 0.1699*	*− 0.1653*	*− 0.1690*	*− 0.1731*
		Py	*− 0.0265*	*− 0.0256*	*− 0.0265*	*0.0128*	*0.0149*	*0.0141*
		Px	0.0259	0.0258	0.0259	0.0052	0.0061	0.0056
	Solvent V, $Å^3$		5122.45			5091.22		
	Volume solvent	Pt	0.0625	0.0634	0.0625	0.0622	0.0637	0.0652
		Pz	*− 0.0609*	*− 0.0619*	*− 0.0609*	*− 0.0620*	*− 0.6341*	*− 0.0650*
		Py	*− 0.0099*	*− 0.0096*	*− 0.0100*	*0.0048*	*0.0059*	*0.0053*
		Px	0.0098	0.0097	0.0102	0.0020	0.0023	0.0021

energy changes show that the main energy shift is concerned with changes of the VdW and HB energies of water molecule structures. It is clearly seen from changes in the extracted water molecules clusters obtained after optimization (Tables 3 and 4, columns 5 and 6). Additionally, changes in the energy result from the formation of new hydrogen bonds of water molecules with inner cavity of D-FF and L-FF (namely with N and O atoms). This result is clearly seen from changes of the binding energy Eb and total energy Et data for water cluster only in their comparison with energies for D-FF and L-FF PNT with water (Tables 3 and 4, columns 4 and 7). In this case, energy changes approximately (both Et and Eb) from − 167.75 to − 87.15 eV (for D-FF case) and from − 164.65 to − 84.43 eV (for L-FF case) are twice higher then for a water cluster only. This means that formation of bonds with the inner surface of a nanotube takes twice as much energy as merely the rearrangement of bonds inside the water cluster.

It is interesting to note that water molecules embedded into a carbon nanotube under the influence of high pressure and temperature lead to a formation of a similar helix structure [59]. It is known that the water confined to nanopores is investigated not only in carbon nanotubes, but in other nanoporous structures, for example, in boron nitride nanotubes (BNNTs) using first-principles calculations [60]. Another study of the polar property, polarization, and even the ferroelectricity in the ice-type (or water-type) nanostructures has recently been performed in nanoporous silicate materials, which have an ordered system of narrow cylindrical pores [61]. It is assumed that in such filamentous pores of the studied materials, ferroelectric ice XI is formed.

We do not yet insist directly on the occurrence of ferroelectricity of water and ice structures inside peptide nanotubes, since reliable phase transitions between the polar (ferroelectric) and nonpolar (paraelectric) phases, which have pronounced changes in the dielectric constant according to the well-known Curie-Weiss law [15], have not yet been detected. Meanwhile, ferroelectricity was observed in [62], though in other β-sheet FF PNT structure [13, 20], not in α-helix, as is studied now [21–25]. Besides, water was not known to occur in the internal cavity of such PNT. This is to be clarified in the future and possible results will be achieved with more detailed dielectric measurements [43], but, otherwise, the presence of such a significant and strictly oriented polarization clearly indicates the possibility of the existence of the ferroelectric-like phenomena here.

Returning to the first important result, it should be noted that the extracted water clusters have helix nanotube structure similar D-FF and L-FF PNT, (but having an inverse chirality sign) and high of dipole moments and corresponding polarizations value directed strongly along nanotube OZ axis: dipole moment of water/ice cluster increases from ~ 1 Debye up to ~ 29 Debye (see Tables 3 and 4). The dipole moment of the whole D-FF and L-FF nanotube with optimized water/ice cluster also increases: it grows from ~ 139.5 Debye up to ~ 158.5 Debye (Tables 3 and 4). It is known from our previous studies [21–25] that empty D-FF and L-FF PNT have high own dipole moment (~ 138–140 Debye) and polarization, determined also by quantum AM1 and PM3 calculations for these structures without water molecules. Similar data are listed in in Tables 3 and 4. A water nanotube acquires such properties under the influence of D-FF and L-FF PNT—it is self-consistent and self-organized process modulated and induced by an electric field from the strongly oriented dipole moments of D-FF and L-FF and their helix structures.

Moreover, if we build longer models of optimized water ice clusters, we get extended needle-shaped strongly polarized ferroelectric-like elements which may have promising potential applications in various fields. As an example, Table 5 shows the results of calculations for more extended water clusters having even higher values of dipole moments and polarization. At the same time, here we presented the calculation data using different methods and we see that RM1 gives the highest values of the dipole moments (up ~ 100 Debye along PNT *c*-axis) and polarization (up ~ 0.174 C/m^2). An important feature is that the value of the perpendicular components Dy and Py has different signs for D-FF and L-FF, corresponding to various orientations of the polar vector in accordance with chirality of PNT.

Polarization of D-FF and L-FF structures with water molecules in cavity is also increases, but their value depends additionaly on the volume of the structure which has a dipole moment (in SI unit polarization is P = 3.33556255*D/V C/m^2). It is noteworthy that in such specific molecular structures, the volume may be determined by various approaches: (1) using Van der Waals surface and (2) using solvent-accessible surface area calculations [34, 63]. Generally, a value of 1.4 Å is used for water as a solvent (because the distances between H_2O molecules in water are known to be ~ 2.76 Å) [34, 64]. In this work, both the volume values were used for polarization calculation (Tables 3, 4, and 5). In principle, the most important is VdW volume for all our cases.

In any case, the polarization obtained, for example, for empty D-FF PNT, has minimum values P ~ 0.06–0.14 C/m^2 (see Table 3, depending of volume used) and corresponding electric field $E = P/(\varepsilon * \varepsilon_0) \sim 1.7$–4.0 GV/m (for $\varepsilon = 4$ [14, 20] and for ε_0—dielectric vacuum constant). Such a strong electric field directed along PNT c-axis inside a cavity induces orientation of each water molecules dipole along this direction (Figs. 5 and 6 f and g, 8, and 9).

In this connection, mention should be made of the work [65], in which water molecules in a carbon nanotube were studied under an applied electric field. It was revealed that under an applied electric field of 1 V/nm = 1 GV/m, water forms a soli D-like structure at all simulation temperatures up to 350 K. The authors of [65] suggest that the electric field induces a phase transition from liquid to ice-nanotube, at

temperatures as high as 350 K, and the electrostatic interaction within the ice-nanotube under an electric field is stronger than that in the absence of an electric field.

Another important point is that after such a treatment of the water cluster inside D-FF and L-FF PNT, this water cluster per se acquires strongly oriented polar properties as a nanosized ferroelectric nanotube. Some manifestations of ferroelectric properties in water structures are known, especially in their nanostructured form in various nanotube types, and under different influences [59–61, 65, 66].

In addition, it should be noted that the straightforward study of ferroelectric phenomena in water and ice tubular and one-dimensionally ordered nanostructures is actively carried out by some research teams. For example, in [66], novel ferroelectric properties of a new form of ice inside single-walled carbon nanotubes were investigated by molecular dynamics simulation. The authors called them "ice nanotubes" (ice NTs) and found them to consist of polygonal water rings stacked one-dimensionally along the nanotube axis. In [66], ice NTs were revealed to show stepwise polarization with a significant hysteresis loop as a function of the external field strength. In particular, pentagonal and heptagonal ice NTs are found to be the world's smallest ferroelectrics with spontaneous polarization of around 1 μC/cm^2 ~ 0.01 C/m^2. This value is on the same order as in our case, but even slightly less—we have, e.g., a polarization value of ~ 0.062–0.133 C/m^2 for D-FF PNT with water/ice cluster and just greater up to ~ 0.05–0.15 C/m^2 in the case of a such ice nanotube alone (and higher for long extended clusters, see in Table 5).

It is significant that the components of both dipole moments and polarization differ here in the direction perpendicular to the main axis of the nanotubes for cases of different chirality. That is, they have different signs for the components Dy, Py for L-FF PNT and D-FF PNT (see also the orientation of the total dipole moment D shown in Fig. 8 and Fig. 9). This exactly corresponds to the formation of the induced (or modulated) helix structure of water clusters of different types of chirality as well. As we showed earlier [21, 24, 25], L-FF molecules form a right-handed helix, and D-FF molecules form a left-handed helix.

According to [66], all these findings show potential applications of nanotube encapsulating dielectric materials for the fabrication of the smallest ferroelectric devices. In turn, we assume that such and similar polar systems based on the tubular ice nanostructures, formed inside peptide nanotubes, have a great future for a variety of applications in many nanodevices.

As is known, ferroelectric properties, in addition to polarization, also represent such a property as piezoelectricity, which has numerous practical applications [15–28]. Recently, it has been shown in [14] that not only FF PNT but also other AA PNT have rather high polarization values and, as a consequence, piezoelectric coefficients. Thus, the results obtained above not only mean that the presence of water/ice structures inside any AA PNT increases and strengthens their polar properties but also have very significant potential opportunities for the development of new types of nanostructures with enhanced piezoelectric properties.

Conclusions

The results obtained allow us to conclude that, on average, after optimizing the water/ice cluster enclosed in the inner hydrophilic cavity of the nanotubes, they acquire strongly anisotropic electrical properties, with significant magnitudes with dipole moments oriented mainly along the axis of the nanotubes. In this case, the average polarization values reach 0.16–0.17 C/m^2 calculated by any methods (the highest values are given by RM1 method, Table 5) along VdW surface.

In conclusion, it must be stated that the main results obtained: (1) after optimization, the embedded water molecular clusters have significantly larger own dipole moments strongly oriented along D-FF and L-FF PNTs channel, while before it did not have such a defined orientation and had a very small dipole moments; (2) the structure organization of this water cluster has very significantly and high change—this water/ice cluster acquires helix properties, with the same helix step as D-FF PNT; and (3) the dipole moment and polarization of the initial empty D-FF and L-FF PNT increased and enhanced after optimization with the presence of the embedded water/ice cluster inside their cavity, particularly with found most optimal 21 H_2O molecular cluster.

Such an obvious and drastic change modulated by the influence of D-FF properties and structural features was established here for the first time using direct modeling and calculations using DFT (VASP) and various semi-empirical quantum methods. Figures 8 and 9 show examples of these effects. This new discovery may lead in the future to the development and emergence of completely unexpected applications and may also serve for the further development of the possibly as yet not entirely clear nanotechnological, medical, and biological breakthroughs.

Acknowledgments This work was partially supported by the Fundacão para a Ciência e a Tecnologia(FCT, Portugal) through project UID/CTM/50025/2013 and UIDB/50011/2020 & UIDP/50011/2020. P.Z. and S.K. are grateful to the FCT (Portugal) through the project "BioPiezo," PTDC/CTM–CTM/31679/2017 (CENTRO-01-0145-FEDER-031679). The computational parts of the study was completed within the framework of the non-commercial Agreement on scientific-technical cooperation between Institute of Mathematical Problems of Biology (IMPB) of the Keldysh Institute of Applied Mathematics RAS (KIAM RAS) and Department of Physics and I3N Institution of the University of Aveiro, Portugal.

Funding This work was supported by Russian Foundation for Basic Research (RFBR No. 19-01-00519-a and No. 18-07-00354-a (S.V. Filippov)).

References

1. Pachahara SK, Subbalakshmi C, Nagaraj R (2017) Formation of nanostructures by peptides. Curr Protein Pept Sci 18(2):1–19
2. Calvin M (1969) Chemical evolution. Molecular evolution, towards the origin of living system on the earth and elsewhere. Claredon, Oxford
3. Yashima E, Ousaka N, Taura D, Shimomura K, Ikai T, Maeda K (2016) Supramolecular helical systems: helical assemblies of small molecules, foldamers, and polymers with chiral amplification and their functions. Chem Rev 116:13752
4. Tverdislov VA (2013) Chirality as a primary switch of hierarchical levels in molecular biological systems. Biophysics 58(1):128–132
5. Mendes AC, Baran ET, Reis RL, Azevedo HS (2013) Self-assembly in nature: using the principles of nature to create complex nanobiomaterials. Wiley Interdiscip Rev Nanomed Nanobiotechnol 5(6):582–612
6. Aryaa SK, Solankia PR, Dattab M, Malhotra BD (2009) Recent advances in self- assembled monolayers based biomolecular electronic devices. J Biosensors Bioelectron 24(9):2810–2817
7. Naaman R, Waldeck DH (2015) Spintronics and chirality: spin selectivity in electron transport through chiral molecules. Annu Rev Phys Chem 66:263–281
8. Silva RF, Araújo DR, Silva ER, Ando RA, Alves WA (2013) L-diphenylalanine microtubes as a potential drug-delivery system: characterization, release kinetics, and cytotoxicity. Langmuir 29(32):10205–10212
9. Emtiazi G, Zohrabi T, Lee LY, Habibi N, Zarrabi A (2017) Covalent diphenylalanine peptide nanotube conjugated to folic acid/magnetic nanoparticles for anti-cancer drug delivery. J Drug Delivery Sci Technol 41:90–98
10. Orsi M (2018) Molecular simulation of self-assembly. In: Azevedo HS, da Silva RMP (eds) Self-assembling Biomaterials. 1st Edition. Molecular Design, Characterization and Application in Biology and Medicine. Woodhead Publishing Series in Biomaterials; Elsevier Ltd.: Amsterdam, The Netherlands, 2018; pp. 305–318
11. Lee OS, Stupp SI, Schatz GC (2011) Atomistic molecular dynamics simulations of peptide amphiphile self-assembly into cylindrical nanofibers. J Am Chem Soc 133(10):3677–3683
12. Brandon CJ, Martin BP, McGee KJ, Stewart JJP, Braun-Sand SB (2015) An approach to creating a more realistic working model from a protein data bank entry. J Mol Model 21(1):11
13. Lehninger AL (1972) Biochemistry. The molecular basis of cell structure and function. Worth, New York
14. Bystrov VS, Bdikin IK, Singh B (2020) Piezoelectric and ferroelectric properties of various amino acids and tubular dipeptide nanostructures: molecular modeling. Nanomater Sci Eng 2(1):11–24
15. Lines ME, Glass AM (1977) Principles and applications of ferroelectrics and related materials. Clarendon Press, Oxford
16. Bystrov VS, Bdikin I, Heredia A, Pullar RC, Mishina E, Sigov A, Kholkin AL (2012) Piezoelectricity and Ferroelectricity in biomaterials: from proteins to self-assembled peptide nanotubes. In: Ciofani G, Menciassi A (eds) Piezoelectric nanomaterials for biomedical applications. Springer, Berlin, pp 187–211
17. Bystrov VS, Seyedhosseini E, Kopyl S, Bdikin IK, Kholkin AL (2014) Piezoelectricity and ferroelectricity in biomaterials: molecular modeling and piezoresponse force microscopy measurements. J Appl Phys 116(6):066803. https://doi.org/10.1063/1.4891443
18. Kholkin A, Amdursky N, Bdikin I, Gazit E, Rosenman G (2010) Strong piezoelectricity in bioinspired peptide nanotubes. ACS Nano 4:610–614
19. Nguyen V, Zhu R, Jenkins K, Yang R (2016) Self-assembly of diphenylalanine peptide with controlled polarization for power generation. Nat Commun 7:13566
20. Bystrov VS, Paramonova EV, Bdikin IK, Kopyl S, Heredia A, Pullar RC, Kholkin AL (2012) Bioferroelectricity: diphenylalanine peptide nanotubes computational modeling and ferroelectric properties at the nanoscale. Ferroelectrics 440(1):3–24
21. Bystrov VS, Zelenovskiy PS, Nuraeva AS, Kopyl S, Zhulyabina OA, Tverdislov VA (2019) Molecular modeling and computational study of the chiral-dependent structures and properties of the self-assembling diphenylalanine peptide nanotubes. J Mol Model 25:199. https://doi.org/10.1007/s00894-019-4080-x
22. Bystrov VS, Kopyl SA, Zelenovskiy P, Zhulyabina OA, Tverdislov VA, Salehli F, Ghermani NE, Vya S, Kholkin AL (2018) Investigation of physical properties of diphenylalanine peptide nanotubes having different chiralities and embedded water molecules. Ferroelectrics 525:168–177. https://doi.org/10.1080/00150193.2018.14328
23. Bdikin I, Bystrov VS, Delgadillo I, Gracio J, Kopyl S, Wojtas M, Mishina E, Sigov A, Kholkin AL (2012) Polarization switching and patterning in self-assembled peptide tubular structures. J Appl Phys 111:074104
24. Bystrov VS, Zelenovskiy PS, Nuraeva AS, Kopyl S, Zhulyabina OA, Tverdislov VA (2019) Chiral peculiar properties of self-organization of diphenylalanine peptide nanotubes: modeling of structure and properties. Math Biol Bioinform 14(1):94–124. https://doi.org/10.17537/2019.14
25. Zelenovskiy PS, Nuraeva AS, Kopyl S, Arkhipov SG, Vasilev SG, Bystrov VS, Gruzdev DA, Waliszek M, Svitlyk V, Shur VY, Marfa L, Kholkin AL (2019) Chirality-dependent growth of self-assembled diphenylalanine microtubes. Cryst Growth Des 19:6414–6421. https://doi.org/10.1021/acs.cgd.9b00884
26. Filippov SV, Bystrov VS (2020) Visual-differential analysis of structural features of internal cavities of two chiral forms of diphenylalanine nanotubes. Biophysics 65(3):1–8
27. Zelenovskiy PS, Vya S, Nuraeva AS, Vasilev SG, Vasileva DS, Alikin DO, Chezganov DS, Krasnov VP, Kholkin AL (2015) Morphology and piezoelectric properties of diphenylalanine microcrystals grown from methanol-water solution. Ferroelectrics 475:127–134
28. Zelenovskiy P, Kornev I, Vasilev S, Kholkin A (2016) On the origin of the great rigidity of self-assembled diphenylalanine nanotubes. Phys Chem Chem Phys 18(43):29681–29685
29. Görbitz CH (2001) Nanotube formation by hydrophobic dipeptides. Chem Eur J 7:5153–5159
30. Görbitz CH (2018) Hydrophobic dipeptides: the final piece in the puzzle. Acta Cryst B74:311–318
31. Kim J, Han TE, Kim Y et al (2010) Role of water in directing diphenylalanine assembly into nanotubes and nanowires. Adv Mater 22:583–587
32. Andrade-Filho T, Martins TC, Ferreira FF, Alves WA, Rocha AR (2016) Water-driven stabilization of diphenylalanine nanotube structures. Theor Chem Accounts 135:185
33. Ryan H, Carter M, Stenmark P, Stewart JJ, Braun-Sand SB (2016) A comparison of X-ray and calculated structures of the enzyme MTH1. J Mol Model 22(7):1–18
34. Hypercube Inc (2010) HyperChem (versions 8.0). Hypercube Inc., Gainesville. http://www.hyper.com/?tabid=360 (accessible March 2018 – May 2020)
35. The Cambridge Crystallographic Data Centre (CCDC). https://www.ccdc.cam.ac.uk/ (accessed July 2018 – May 2020) Crystallographic data for D-FF nanotubes structure reported in [21, 25] have been deposited in the Cambridge Crystallographic

Data Centre, no. CCDC 1853771; and Crystallographic data for L-FF reported in [29] – is correspond to No. CCDC 16337
36. VASP (Vienna Ab initio Simulation Package), [https://www.vasp.at/] (Accessed July 2019 — May 2020)
37. Kresse G, Furthmüller J (1996) Efficient iterative schemes for *ab initio* total-energy calculations using a plane-wave basis set. Phys Rev B Condens Matter Mater Phys 54:11169–11186. https://doi.org/10.1103/PhysRevB.54.11169
38. Kresse G, Joubert D (1999) From ultrasoft pseudopotentials to the projector augmented-wave method. Phys Rev B Condens Matter Mater Phys 59:1758–1775
39. Perdew JP, Burke K, Ernzerhof M (1996) Generalized gradient approximation made simple. Phys Rev Lett 77:3865–3868
40. Paier J, Hirschl R, Marsman M, Kresse G (2005) The Perdew-Burke-Ernzerhof exchange-correlation functional applied to the G2-1 test set using a plane-wave basis set. J Chem Phys 122:234102
41. Blöchl PE (1994) Projector augmented-wave method. Phys Rev B Condens Matter Mater Phys 50:17953–17979
42. Grimme S, Antony J, Ehrlich S, Krieg S (2010) A consistent and accurate ab initio parametrization of density functional dispersion correction (dft-d) for the 94 elements H-Pu. J Chem Phys 132:154104
43. Bystrov V, Coutinho J, Zelenovskiy P, Nuraeva A, Kopyl S, Zhulyabina O, Tverdislov V (2020) Structures and properties of the self-assembling diphenylalanine peptide nanotubes containing water molecules: modeling and data analysis. Nanomaterials 10:1999; issued 10.10.2020. https://doi.org/10.3390/nano10101999
44. Monkhorst HJ, Pack JD (1976) Special points for Brillouin-zone integrations. Phys Rev 13:5188–5192
45. Morrison I, Li J-C, Jenkins S, Xantheas SS, Payne MC (1997) Ab-initio total energy studies of the static and dynamical properties of ice Ih. J Phys Chem B 101:6146–6150
46. Wang L, Zhao J, Li F, Fang H, Lu JP (2009) First-principles study of water chains encapsulated in single-walled carbon nanotube. J Phys Chem C 113:5368–5375
47. Yang R, Hilder TA, Chung SH, Rendell A (2011) First-principles study of water confined in single-walled silicon carbide nanotubes. J Phys Chem C 115(17):255–264
48. Pople JA, Beveridge DL (1970) Approximate molecular orbital theory. McGraw-Hill, New York
49. Murrell JN, Harget AJ (1971) Semi-empirical self-consistent-field molecular orbital theory of molecules. Wiley Interscience, New York
50. Dewar MJS, Zoebisch EG, Healy EF, Stewart JJP (1985) Development and use of quantum mechanical molecular models. 76. AM1: a new general purpose quantum mechanical molecular model. J Am Chem Soc 107:3902
51. Dewar MJS, Dieter KM (1986) Evaluation of AM1 calculated proton affinities and deprotonation enthalpies. J Am Chem Soc 108:8075
52. Stewart JJP (1990) MOPAC: A semiempirical molecular orbital program. J Comp Aided Mol Design 4:1
53. Stewart JJP (1989) Optimization of parameters for semiempirical methods. I. Method. J Comput Chem 10:209
54. Stewart JJP (1989) Optimization of parameters for semiempirical methods. II. Applications. J Comput Chem 10:221
55. Stewart JJP (2007) Optimization of parameters for semiempirical methods V: modification of NDDO approximations and application to 70 elements. J Mol Model 13(12):1173–1213
56. Rocha GB, Freire RO, Simas AM, Stewart JJP (2006) RM1: a Reparameterization of AM1 for Y, C, N, O, P, S, F, Cl, Br, and I. J Comput Chem 27(10):1101–1111
57. Lima NBD, Rocha GB, Freire RO, Simas AM (2019) RM1 semi-empirical model: chemistry, pharmaceutical research, molecular biology and materials science. J Braz Chem Soc 30(4):10.21577/0103-5053.20180239
58. Müller U (2013) Symmetry relationships between crystal structures. Applications of crystallographic group theory in crystal chemistry. Oxford University Press, Oxford
59. Bai J, Wang J, Zeng XC (2006) Multiwalled ice helixes and ice nanotubes. Proc Natl Acad Sci U S A 103(52):19664–19667
60. Shayeganfar F, Beheshtian J, Shahsavari R (2018) First-principles study of water nanotubes captured inside carbon/boron nitride nanotubes. Langmuir 34(37):11176–11187
61. Bordonskiy GS, Orlov AO (2014) The study of ferroelectric phase transitions of water in nanoporous silicates with joint electrical noise and calorimetric measurements. Phys Solid State [Physica Tverdogo Tela] 56(8):1575–1582 (in Russian)
62. Bdikin I, Bystrov V, Kopyl S et al (2012) Evidence of ferroelectricity and phase transition in pressed diphenylalanine. Appl Phys Lett 100:043702. https://doi.org/10.1063/1.3676417
63. Bodor N, Gabanyi Z, Wong C (1989) A new method for the estimation of partition coefficient. J Am Chem Soc 111:3783
64. Gavezotti A (1983) The calculation of molecular volumes and the use of volume analysis in the investigation of structured media and solid-state organic reactivity. J Am Chem Soc 105:5220
65. Winarto W, Yamamoto E, Yasuoka K (2017) Water molecules in a carbon nanotube under an applied electric field at various temperatures and pressures. Water 9(7):473
66. Mikami F, Matsuda K, Kataura H, Maniwa Y (2009) Dielectric properties of water inside single-walled carbon nanotubes. ACS Nano 3(5):1279–1287